Intersystem crossing as a key component of the non-adiabatic relaxation dynamics of bithiophene and terthiophene

Thomas Schnappinger,[†] Marco Marazzi,[‡,¶] Sebastian Mai,[§] Antonio Monari,[¶] Leticia González,[§] and Regina de Vivie-Riedle[*,†]

Department of Chemistry, Ludwig-Maximilians-Universität München, D-81377 München, Germany, Departamento de Química, Centro de Investigación en Síntesis Química (CISQ), Universidad de La Rioja, 26006 Logroño, Spain, Université de Lorraine and CNRS, LPCT UMR 7019, F-54000 Nancy, France, and Institute of Theoretical Chemistry, Faculty of Chemistry, University of Vienna, 1090 Vienna, Austria

E-mail: Regina.de_Vivie@cup.uni-muenchen.de

Abstract

We present a non-adiabatic dynamics study concerning the sub picosecond relaxation of excited states in dimeric and trimeric thiophene chains. The influence of the triplet states in the overall process is, for the first time, taken into account by explicitly including spin-orbit couplings and hence allowing intersystem crossing phenomena. We observe the fundamental role of the triplet state manifold in driving the full relaxation

---

[*]To whom correspondence should be addressed
[†]Department of Chemistry, Ludwig-Maximilians-Universität München, D-81377 München, Germany
[‡]Departamento de Química, Centro de Investigación en Síntesis Química (CISQ), Universidad de La Rioja, 26006 Logroño, Spain
[¶]Université de Lorraine and CNRS, LPCT UMR 7019, F-54000 Nancy, France
[§]Institute of Theoretical Chemistry, Faculty of Chemistry, University of Vienna, 1090 Vienna, Austria

process. In particular we evidence the effect of both, inter-ring rotation and ring-opening, in the process, as compared to the monomer, where the ring-opening process appears as the dominant one. In addition, the evolution of the open structures allows for *trans* to *cis* isomerization in the dimer and trimer. The overall relaxation process slows down with chain elongation. The complex decay mechanism characterized by the presence of different competing channels, due to the presence of a quasi degenerate manifold, is explained allowing the rationalization of oligothiophenes photophysics.

Introduction

Due to their remarkable intrinsic properties thiophene derivatives and their oligomers are promising candidates to be employed in organic materials for technological applications.[1,2] They undergo rapid intersystem crossing (ISC)[3–5] leading to extremely high triplet quantum yields.[6] This property deviates strongly from the common behavior found in most organic molecules where the ratio of ISC to internal conversion (IC) and fluorescence is rather small.[7] Also, it is important for charge separation and transport in conductive organic materials. In combination with their efficient light harvesting and structural versatility they have attracted much attention as building blocks for photoactive polymers and molecular aggregates. Examples are solar cells,[8–12] light emitting diodes,[13,14] photoswitches[15] and biological labels.[16–18] In addition, polythiophene bridges are also used to enhance two-photon absorption cross sections.[19–21] As poly(3-hexylthiophene) (P3HT) they form in combination with phenyl-C61-butyric acid methyl ester (PCBM) the famous P3HT/PCBM solar cell.[11,22]

A deeper understanding of the initial processes after photoexcitation and the subsequent relaxation mechanisms of oligothiophenes is essential to improve the performance of thiophene-based applications. In our previous works[23,24] we were able to explain the relaxation processes for the monomer thiophene with the aid of static quantum chemical calculations and non-adiabatic molecular dynamics simulations: after photoexcitation, fast ring-opening (approx. 100 fs) leads to a degeneracy of singlet and triplet states. This degeneracy and the

corresponding flat potential energy surface traps the system in entropically favored open-ring structures in the singlet as well as in the triplet states (up to 50 ps).[25]
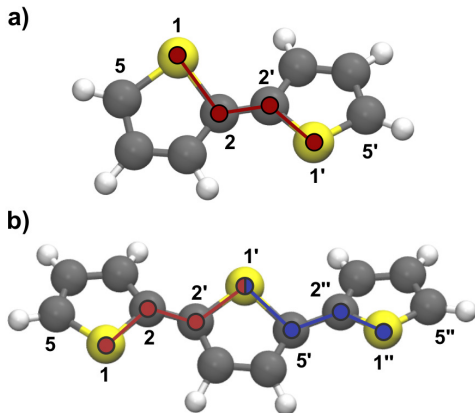
Figure 1: Structure of 2,2'-bithiophene (TP2) in the *trans* conformation a) and of 2,2':5',2''-terthiophene (TP3) in the *eclipsed-anti-anti* (*eAA*) conformation b). All relevant atoms are labeled, as well as the inter-ring dihedral angles: Φ_{SCCS} (red) in TP2, Φ_{SCCS}^1 (red) and Φ_{SCCS}^2 (blue) in TP3, respectively. The nomenclature is explained in more detail in the Supporting Information (SI[†]).

The structures of the most stable conformer are shown in Figure 1 for the dimer TP2 (2,2'-bithiophene) and the trimer TP3 (2,2':5',2''-terthiophene). For both TP2 and TP3 experimental results[6,26–28] indicate that ultrafast ISC takes place from the first excited singlet state. Moreover experimental and theoretical studies suggested two ISC channels for both systems with timescale ranging from 1 ps up to 140 ps.[26,27] Based on static quantum chemical calculations[23,29? –32] and dynamics simulations (excluding triplet states)[33,34] the relaxation processes after photo excitation for TP2 and TP3 are mainly ascribed to the torsional motion around the quite flexible inter-ring bonds,[35] whereas ring-opening via CS-bond cleavage should only play a minor role in the initial relaxation processes of both systems. However, for the previous dynamics simulations[33,34] only short simulation times (300-500 fs) were studied and important ISC processes were excluded.

This work presents the first non-adiabatic dynamical study of the dimer TP2 and the trimer TP3 at picosecond timescale explicitly including spin-orbit couplings and triplet states. For this study we have used the surface hopping including arbitrary couplings (SHARC) soft-

ware package,[36–39] which has already been successfully applied to an important number of molecular systems.[24,40–44]

Computational methods

Ab initio level of theory

The electronic states of TP2 and TP3 were computed using the density functional theory (DFT) and linear response time dependent DFT (LR-TDDFT). All LR-TDDFT calculations have been performed within the so-called Tamm-Dancoff approximation (TDA).[45] The DFT and TDA calculations were carried out with the ADF program package (version 2017),[46,47] using the B3LYP[48–50] exchange-correlation functional with the D3 dispersion correction by Grimme and coworkers.[51] Minima (Min), transition states (TS), conical intersections (CoIn) and singlet-triplet minimum-energy crossings (STC) were optimized with the ORCA code (version 3.0.3)[52] as an external optimizer. All optimized geometries are given in the Supporting Information (SI†). The DFT and TDA calculations were carried out with the the double zeta polarized basis set (DZP)[53] and a Becke[54,55] and Zlmfit[56] grid of good quality. For benchmarking purposes, some calculations were performed with the triple zeta polarized basis set (TZP)[53] in combination with the same grid quality. In all optimization calculations symmetry was not used. Scalar relativistic effects were included with the zeroth-order regular approximation (ZORA),[57–61] and the spin-orbit couplings (SOC) were calculated using a perturbative method, as developed and implemented by Wang and Ziegler.[62]

Dynamics

The molecular dynamics of TP2 and TP3 were simulated using the SHARC *ab initio* dynamics package version 2.0.[36–39] The necessary energies, gradients, non-adiabatic couplings and spin-orbit couplings were calculated on-the-fly at the TDA/B3LYP level of theory. The initial conditions for the dynamics simulations were generated based on a Wigner distri-

bution computed from harmonic vibrational frequencies in the optimized ground state equilibrium geometry. The underlying frequency calculations were performed at B3LYP/DZP level of theory. For TP2 only the *trans* conformer was studied, since it has been shown to be the ground state global minimum.[23,63] Time-resolved spectroscopic studies on the dimer[26,27] used an excitation energy of 4.02 eV to reach the rising edge of the first absorption peak. Corresponding to these experiments we have centered the spectral window (3.0-4.0 eV) at the rising edge of the first absorption peak (see the simulated absorption spectrum in the SI[†]). 84 starting geometries and velocities were stochastically chosen.

For TP3, among the total number of ten ground state minima,[31,64?–66] two nearly isoenergetic minima exist.[23] The *eclipsed-anti-anti* (*eAA*) conformer is the global minimum and the *gauche-anti-anti* (*gAA*) conformer is only 0.02 eV (ΔG)[23] above. Since these conformers can easily interconvert, as will be shown below, we restrict our initial condition generation to the *eAA* conformer. For the dynamics simulations of TP3, 36 starting geometries and velocities in the energy window 3.0-4.0 eV were stochastically chosen from a Wigner distribution (see the simulated absorption spectrum in the SI[†]). For both systems, in accord with the chosen excitation window, all trajectories started in the S_1 state.

The SHARC *ab initio* surface-hopping algorithm uses a fully diagonal, spin-mixed electronic basis, resulting from the diagonalization of the Hamiltonian containing spin-orbit couplings.[37,67] The integration of the nuclear motion is done with the Velocity-Verlet algorithm with a maximal time of 1 ps using a time step of 0.5 fs. In each time step, gradients were computed for all states which are closer than 0.2 eV to the active state; this is required in order to construct the gradient of the spin-mixed active state. The coefficients of the electronic wavefunction are propagated on interpolated intermediates with a time step of 0.02 fs applying a local diabatization technique[68] in combination with the WFoverlaps code[69] to compute the wave function overlaps. Decoherence correction was taken into account using the energy-based method of Granucci and Persico with the parameter $\alpha = 0.1$ a.u.[70]

For the statistical analysis of the results stemming from the non-adiabatic dynamics, the

number of aborted trajectories has to be considered. Some trajectories experienced convergence problems and therefore terminated before reaching 1 ps. Beside the convergence, also problems arising from the DFT/TDA methodology (e.g. the multi-configurational character of the ground state) have to be taken into account since they may lead to unphysical behavior of the energy and the gradients. In order to find a good compromise between the simulation time considered and the number of trajectories inspected, we restrict our analysis to trajectories with at least 400 fs of simulation time, a maximum change in the total energy of 0.2 eV, a maximum change in the total energy per step of 0.2 eV and a maximal inter-state hop energy of 1.0 eV.

Results and discussion

Validation of the level of theory

First, it was checked whether the static B3LYP/DZP and B3LYP/TZP results for both systems are in qualitative agreement with previous CASPT2 results[23] and the experimental data.[6,32,71–73] Therefore, the excitation energies of the optimized ground-state minima (*trans* for TP2 and *eAA* for TP3) were benchmarked (see Table 1).

The calculated S_1 and S_2 excitation energies for TP2 are in between the CASPT2 and the experimental results. For the first four triplet states the B3LYP energies are in good agreement with the CASPT2 values. The energetic order and the electronic character of all tested states are the same as in previous studies.[23,29,30,32] Moreover, the B3LYP functional reproduces the CASPT2 excitation energies for the first six states of TP3 quite well. The character of the states is also the same as in previous studies,[23,31,32] except for a slight difference in the state ordering. Using TDA the third triplet state T_3 lies above the S_1 independently of the chosen basis set. For both systems the TZP basis set gives better agreement with experiment than the smaller basis set DZP. In order to save time for the dynamics simulations we decided to use the small DZP basis set, as it is sufficient to well

Table 1: Calculated vertical singlet and triplet excitation energies (eV) for the low-lying excited states at the optimized ground-state minimum of TP2 and TP3 compared to experimental and theoretical data. Oscillator strength values are given in parentheses. Energies were calculated using B3LYP/DZP and B3LYP/TZP.

TP2 State	Char.	B3LYP/DZP	B3LYP/TZP	CASSCF[a]	CASPT2[b]	Exp.
S_1	$\pi_1 \rightarrow \pi_1^*$	4.50 (0.54)	4.24 (0.48)	6.44 (0.45)	4.51 (0.45)	4.29[c]
S_2	$\pi_1 \rightarrow \pi_2^*$	5.07 (0.01)	4.94 (0.00)	5.87 (0.01)	4.85 (0.01)	5.08[c]
T_1	$\pi_1 \rightarrow \pi_1^*$	3.01	2.76	2.94	2.86	2.32[d]
T_2	$\pi_1 \rightarrow \pi_2^*$	4.00	3.95	3.94	3.82	-
T_3	$\pi_2 \rightarrow \pi_1^*$	4.28	4.11	5.08	4.41	-
T_4	$\pi_3 \rightarrow \pi_1^*$	4.32	4.22	4.91	4.48	-
TP3 state	Char.	B3LYP/DZP	B3LYP/TZP	CASSCF[e]	CASPT2[f]	Exp.
S_1	$\pi_1 \rightarrow \pi_1^*$	3.81 (0.52)	3.46 (0.49)	5.84 (0.47)	4.03 (0.55)	3.50[g]
S_2	$\pi_2 \rightarrow \pi_1^*$	4.37 (0.00)	4.10 (0.00)	4.77 (0.00)	4.42 (0.00)	-
T_1	$\pi_1 \rightarrow \pi_1^*$	2.59	2.21	2.51	2.40	1.90[d]
T_2	$\pi_1 \rightarrow \pi_2^*$	3.40	3.15	3.34	3.19	2.99[d]
T_3	$\pi_1 \rightarrow \pi_3^*$	4.00	3.81	4.05	3.85	-
T_4	$\pi_3 \rightarrow \pi_1^*$	4.08	4.00	4.81	4.30	-

[a] CASSCF(12/11)/6-31G* underlying results from reference;[23]
[b] CASPT2(12/11)/6-31G*;[23] [c] Gas-phase absorption spectrum at room temperature;[71]
[d] Photodetachment photoelectron spectrum in the gas phase;[32]
[e] CASSCF(18/15)/6-31G*[23] underlying results from reference;[23]
[f] CASPT2(18/15)/6-31G*;[23] [g] Absorption spectrum in solution at room temperature.[6,72,73]

describe the low-lying excited excited states of TP2 and TP3 in the Franck-Condon region. In contrast to the CASPT2 methodology the excitation energies at the CASSCF level as well as the state ordering is wrong for TP2 and TP3. Hence, a meaningful description of TP2 and TP3 is not possible using CASSCF.

Based on static quantum chemical calculations[23,29–32] two possible deactivation pathways for TP2 and also TP3 were discussed: the first pathway is described by the rotation around the inter-ring bonds. This rotation leads to a near-degeneracy region of triplet states and the S_1 state. In combination with the moderate spin-orbit couplings this degeneracy should allow ISC; subsequent internal conversion steps lead the system in the T_1 state. The relaxation back to the ground state can take place through either phosphorescence or non-radiative processes like cleavage of a C-S bond. The second pathway is similar to the relaxation mech-

anism in the thiophene monomer:[24] the C-S bond cleavage leads to open-ring structures where the S_0, T_1, S_1 and T_2 states are nearly degenerate and the SOC increases significantly. Via these open-ring structures, closed-ring conformers can be formed in the ground state. In principle for TP2 as well as for TP3 many open-ring structures are possible. As shown in our previous work[23] structures with only one broken C-S bond are energetically favored. In TP2 the four C-S bonds can be distinguished into two groups: the *inner* bonds (1,2 and 1',2', see Fig. 1) and the *outer* bonds (1,5 and 1',5'). The cleavage of the *inner* bonds is energetically favored. The C-S bonds of TP3 can be distinguished analogously in three groups: for both terminal rings the C-S bonds can be divided into *inner* and *outer* ones. The C-S bonds of the central thiophene ring form the third group, the *central* bonds. The cleavage of one of the *inner* or *central* bonds leads again, compared to *outer* bonds, to more stable structures. In the following the discussion is restricted to open-ring structures with a single broken *inner* or *central* C-S bond.

All critical points of TP2 and TP3 along both relaxation pathways were optimized using the small basis set DZP. The excitation energies of the six low-lying excited states were determined and compared with previous CASPT2 calculations.[23] These results are collected in the SI†. For all closed-ring structures the B3LYP/DZP results are in sufficient agreement with the CASPT2 values with slightly higher deviations for open-ring structures. We are aware of the inherent problems of the TD-DFT methodology to describe multi-configurational character in the ground-state and conical intersection between S_1/S_0. However, in previous studies on oligothiophenes[23,32–34] the relaxation pathway can be split into two parts. In the first part describing the path from the Franck-Condon region to the open-ring structures the triplet states lie energetically close to the S_1 state and the spin-orbit coupling is large. We are very confident that this first part of the relaxtion is fully described by TD-DFT. The second part is the dynamic of the open-ring structures and the relaxation back to the ground-state. Here the conical intersection between S_1/S_0 is very important but not described well using TD-DFT. This may be biasing the simulation towards the triplet state population. On the

other hand, the relaxation into triplet states is also present in thiophene where we could perform the dynamics simulation at the CASSCF level.[24] Nevertheless, the overall shape of the potential energy surfaces along the pathways is qualitatively well reproduced using the B3LYP/DZP methodology. Therefore, we are convinced that the chosen methodology is adequate to describe the dynamics of TP2 and TP3.

Excited state dynamics of 2,2'-bithiophene (TP2)

Using our selection criteria, 53 trajectories out of 84 trajectories were taken into account to analyze the excited state dynamics of TP2. These 53 trajectories were first analyzed according to the final populated state and the final molecular geometry.A geometry is characterized as open-ring structure if one of the C-S bonds is larger than 2.4 Å. The results are summarized in Table 2.

Table 2: Distribution (%) of the TP2 B3LYP/DZP trajectories according to the final populated state as well as the final geometry. All percentages are given with respect to the total number of analyzed trajectories. The shown numbers are statistically not fully converged. The maximum statistical error is 13 %.[74]

final state	final geometry			Σ
	open	cis	trans	
S_0	16	12	6	34
S_1	4	0	0	4
T_1	24	4	10	38
T_2	24	0	0	24
Σ	68	16	16	100

After excitation to the S_1 state, all analyzed trajectories show non-adiabatic relaxation within the first picosecond. The final distribution between the singlet and the triplet states is nearly 2:3. Within the triplet manifold the relative distribution T_1:T_2 is about 3:2, within the singlet moiety S_0:S_1 is 8.5:1. Most final geometries are open-ring structures (68 %), where one *inner* bond is broken. Closed-ring conformations (*trans* or *cis*) are only found for the S_0 and the T_1 state. Note that in the monomer almost no triplet closed-ring structures were found.[24] Although all trajectories have been propagated from an initial *trans* conformation,

a one-to-one mixture of *trans* and *cis* conformers is observed after relaxation.

The overall change in population of the ground state and the individual excited states for the first picosecond is shown in Figure 2 for the TP2 dynamics.
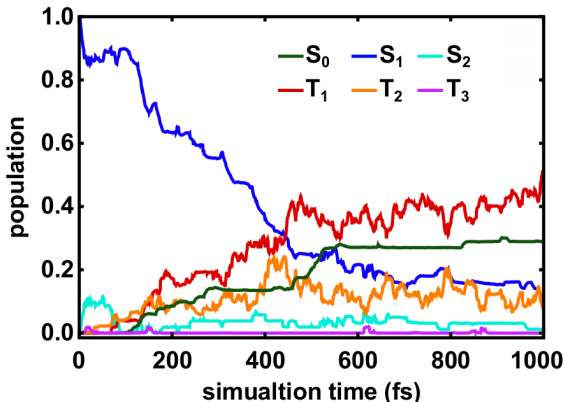
Figure 2: Time evolution of the average populations along the TP2 trajectories. The ground and the five lowest excited states are displayed.

The populations dynamics of TP2 is more complex than for the thiophene monomer[24] and far from exponential behavior. It is characterized by a fast decay of the S_1 state population. In the first 3 to 5 fs there is an ultrafast exchange of some population between S_1 and S_2 states, probably attributable to the initial conditions. Nevertheless, during the whole process the S_2 state plays no role. Indeed, after this initial exchange, the S_1 state population stays constant for about 100 fs. Thereafter the first two triplet states, T_2 and T_1, start to participate via ISC. The S_1 state is mainly depopulated via the T_2. Subsequently the T_1 state is populated via IC. This cascade $S_1 \rightarrow T_2 \rightarrow T_1$ finally enables the population transfer back in the ground state S_0. The T_3 state is nearly not populated. The ratio between S_0, S_1, T_1 and T_2 after 1 ps simulation time is approx. 30 : 10 : 50 :10. Compared to the monomer dynamics, the relaxation from S_1 state is significantly slower in the first 200 fs.

Next we analyze which relaxation pathway leads to the final structures. The two most relevant internal coordinates, previously introduced, are the rotation around the inter-ring bond (i.e. the dihedral angle Φ_{SCCS}) and the C-S bond cleavage described as the averaged C-S distance r_{CS} of both *inner* C-S bonds. In Figure 3 the time evolution (color coded) of

10

the trajectories is shown for the first 200 fs.
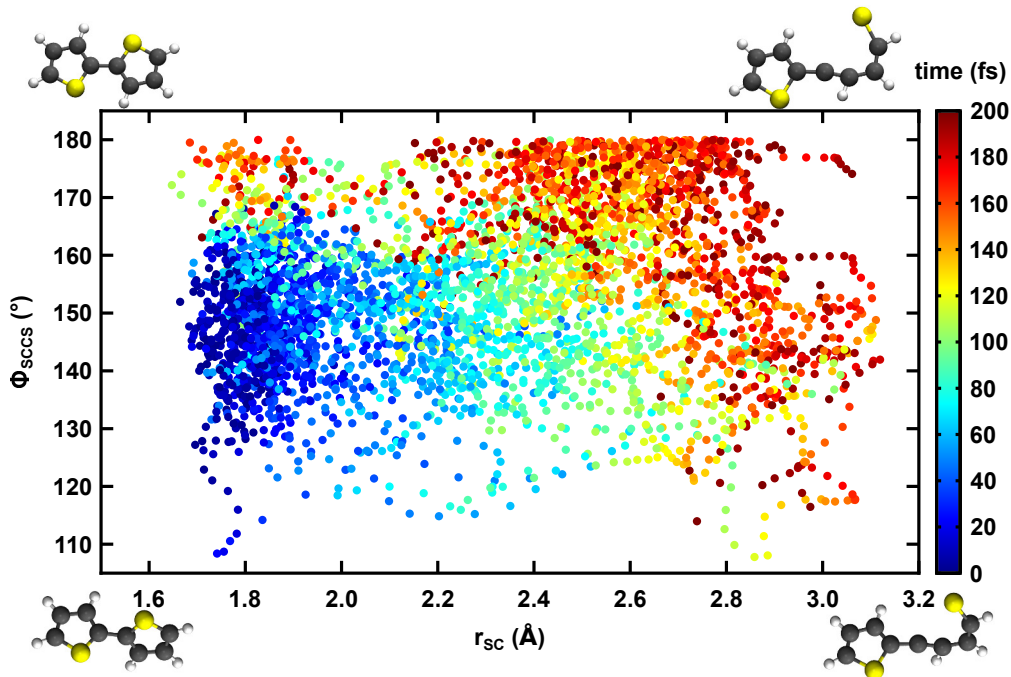
Figure 3: Analysis of the non-adiabatic dynamics of TP2 within the first 200 fs. Time evolution (see color code) of the trajectories in the subspace spanned by the averaged 'inner' C-S distance r_{CS} and the dihedral angle Φ_{SCCS}.

Starting from the Wigner distribution (dark blue dots) the dihedral angle Φ_{SCCS} varies between 130° and 160° (S$_0$-minimum at 143.0°) and an averaged *inner* C-S distance r_{CS} is found between 1.7 Å and 1.9 Å (S$_0$-minimum value 1.75 Å). Within the first 100 fs a small part of the trajectories leads to planarization while the majority undergoes ring-opening reaching an average bond distance of up to 2.6 Å. Thereafter further bond elongation is accompanied by significant planarization reaching 180°. The dynamics simulation shows that both reaction coordinates (ring-opening and planarization) are active on the same time scale. The energetic barrier for the ring-opening in TP2 is estimated to be 0.2 eV (B3LYP/DZP). The maximal barrier at CCSD/6-31G* level of theory was found to be 0.4 eV.[23] Both values are higher than for the barrier in the monomer[24] found at 0.1 eV. Our dynamics simulations confirm that due to the excess kinetic energy deposited in the photon absorption process this barrier can still be overcome, but it explains the slower decay of the S$_1$ population (see

Fig. 2). The complete temporal evolution up to 1 ps for Φ_{SCCS} and r_{CS} can be found in the SI[†].
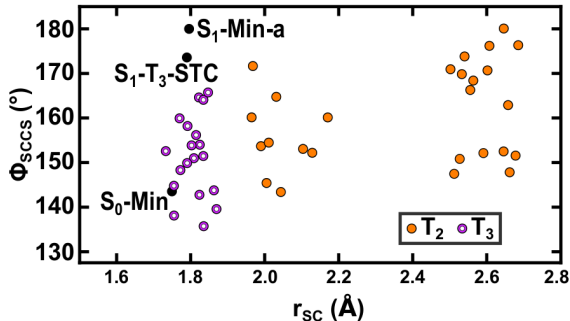
Figure 4: Locations of the geometries where the first surface hops from the S_1 state to triplet states (T_2 and T_3) occurred depending on r_{cs} and Φ_{SCCS} in TP2 within the first 200 fs. The hopping geometries are displayed in different colors according to the target state of the hopping event. Additionally, relevant B3LYP/DZP optimized geometries are represented in black, including minima (Min) and singlet-to-triplet crossings (STC).

The geometrical deformations observed in the first 200 fs lead to many intersystem crossing events from the S_1 state into the triplet states (see Fig. 4). Mostly transitions into the T_2 and T_3 state are observed, which is in agreement with previous results.[23,34] In principal these hopping events can be distinguished geometrically and temporally. Hops between the S_1 state and the T_3 state only occur for closed-ring and non-planar geometries, hence very early. They are mainly forward and backward hops with no net populations exchange. This explains the plateau in the S_1 state population observed in Figure 2 in the range from 3 up to 100 fs. Hops to the T_2 state are observed around two different r_{CS} values. For the slightly elongated C-S bonds (2.0-2.2 Å) the SOC values increase and the two states T_2 and S_1 cross. This initiates the decay of the S_1 state after 100 fs in Figure 2. Further elongation of r_{CS} (up to 2.5-2.6 Å) leads to a further increase in the SOC and to a near degeneracy of the T_2 and S_1 state, giving rise to a second enhancement of hops shown in Figure 4. A complete analysis of all hopping events for the whole simulation time can be found in the SI[†]. The open-ring dynamics lead, as in the case of the thiophene monomer,[24] to a dynamical equilibrium between singlet and triplet states. All states involved, S_0, S_1, T_1 and T_2, come

12

close in energy accompanied by rather large effective spin-orbit couplings (SI[†]). Although the degeneracy is not as complete among all states as in case of the monomer, many back and forward hops between S_1, T_1 and T_2 establish the dynamical equilibrium. Due to the chosen methodology, i.e. TDDFT, hops back into the ground state are only possible via the T_1 and T_2 state because of a poor description of the open-ring S_1/S_0 conical intersection. This might explain why the final population in S_0 is lower than in T_1, while for the monomer, calculated at CASSCF level, both states were equally populated.[24]

The energy profiles of four illustrative trajectories are shown in Figure 5. The individual states are color coded and the populated state is marked with black diamonds.
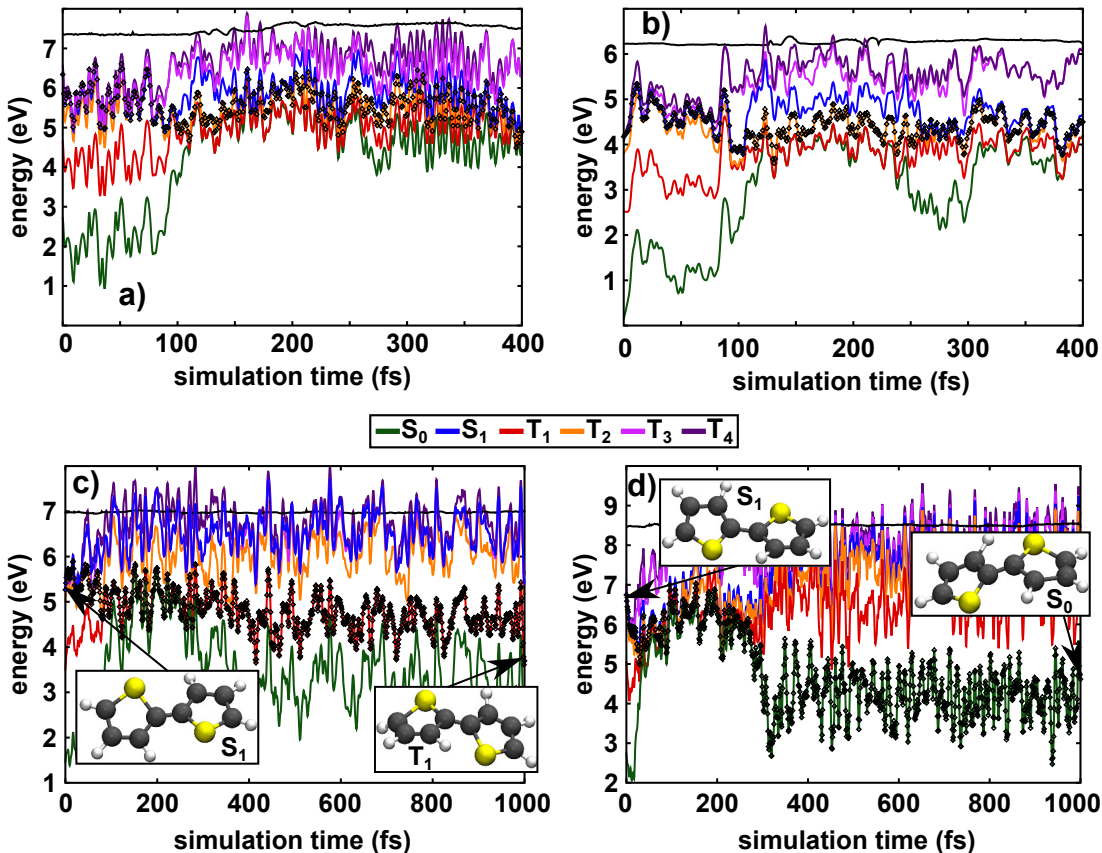
Figure 5: Energy profiles of four representative TP2 trajectories following the ring-opening mechanism. All trajectories were initiated on the S_1 potential energy surface. The time evolution of the ground and the six lowest excited states are displayed in color, whereas the running state is indicated with black diamonds. The energies are plotted relative to the ground state minimum. Initial and final structures are given for the last two trajectories.

All four trajectories undergo ring-opening with the cleavage of one of the *inner* C-S bonds after the first 100 fs. In Figure 5 a) and b) we focus on the first 400 fs. In the open-ring structure, the system switches mostly between the quasi-degenerate S_1 and the T_2 state. In contrast to the monomer case, the ground state S_0 and the first triplet state T_1 show much less participation to the process. Two different reaction pathways leading to closed-ring structures are shown in Figure 5 c) and d). In example c) one C-S bond is broken after approximately 90 fs. The T_1 state is reached via S_1 and T_2 20 fs later. Although the T_1 state and the ground state are nearly degenerate, no hops occur for the next 100 fs and the ring-closure takes place in the triplet state forming a nearly planar *trans* conformer. In contrast, Figure 5 d) reports an example of relaxation to a closed ring *trans* conformer in the S_0 state, reached from the S_1 state via the T_2 and the T_1 state. Note, that although we presented trajectories leading to *trans* products, the open ring structures can rotate almost freely around the inter-ring bond and hence can easily undergo isomerization into the *cis* conformer. This is reflected in the ratio between *trans* and *cis* products shown in Table 2. The amount of closed-ring conformers found for the T_1 state explains the experimentally observed phosphorescence[75] which might occur from these stable geometries.

Excited state dynamics of 2,2':5',2"-terthiophene (TP3)

For TP3, 34 out of 36 trajectories were taken into account for discussion of the excited state dynamics. These 34 trajectories were first analyzed according to the final populated state and the final molecular geometry. Just as for the TP2 analysis a geometry is characterized as open-ring structure if one of the C-S bonds is larger than 2.4 Å. The results are summarized in Table 3.

Overall 62% of the trajectories terminate in the singlet manifold from which only 8.8 % reach the S_0 state. The triplet states are significantly less populated compared to the dimer. The relative distribution of the T_1 and the T_2 state is 8:5, while the T_3 and S_2 states play no role. This is a first hint for an enhanced life time of the S_1 state. For all excited states

Table 3: Distribution (absolute numbers) of the TP3 B3LYP/DZP trajectories according to the final populated state as well as the final geometry. The shown numbers are statistically not fully converged. The maximum statistical error is 17 %.[74]

final state	*inner*	*central*	vib. only^a	e-AA^b	e-SS^b	g-AA^b	g-SA^b	g-SS^b	Σ
					final geometry				
S_0	0	0	0	0	1	1	1	0	3
S_1	5	4	4	2	0	1	0	0	16
S_2	1	1	0	0	0	0	0	0	2
T_1	2	1	0	4	0	0	1	1	9
T_2	1	3	0	0	0	0	0	0	4
Σ	9	9	4	6	1	2	2	1	34

^{a} Only vibrational dynamics observed;
^{b} The nomenclature is explained in the SI†.

the open-ring structures are again dominant (53 %). No significant preference towards the cleavage of the *inner* or the *central* C-S bonds is observed. The sum of the closed-ring structures in the T_1 and S_0 states amount to 35 %, with an excess of the *eAA* conformer. In contrast to the TP2 dynamics, nearly 29 % of the analyzed trajectories stay near the FC-region in the S_1 state, thereof 12 % show only vibrational dynamics.

The time evolution of the populations of the ground state and the individual excited states are shown in Figure 6 for the TP3.
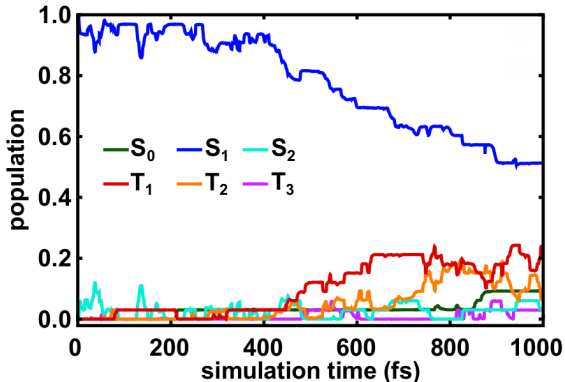
Figure 6: Time evolution of the average populations of the participating excited states for the TP3 trajectories. The ground and the five lowest excited states are displayed.

The relaxation process of the S_1 state is significantly slower than in TP2 and again non-exponential. In the first 400 fs the S_1 population stays nearly constant. The time needed for

15

geometrical rearrangement is thus four times longer than for the dimer. After this period, the first two triplet states (T_2 and T_1) can participate in the dynamics and start the non-adiabatic decays. A cascade $S_1 \to T_2 \to T_1$ enables the population transfer back to the ground state S_0, comparable to the relaxation dynamics in TP2. Again S_2 and T_3 do not participate. The ratio between S_0, S_1, T_1 and T_2 after 1 ps simulation time is approx. 15 : 50 : 25 : 10. The geometrical relaxation process is analyzed with the help of four collective variables associated to ring-opening and the rotation around the inter-ring bonds. The inter-ring rotation is characterized by the two dihedral angles, Φ^1_{SCCS} and Φ^2_{SCCS} (see Fig. 1 b)). The ring-opening is characterized by the averaged CS distance of both *inner* bonds (r^{inner}_{CS}) and of both *central* bonds ($r^{central}_{CS}$). The time evolution of these variables is shown in Figure 7.
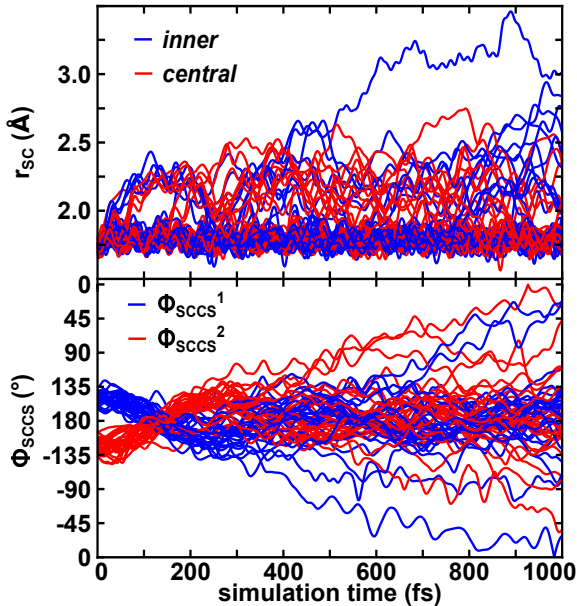
Figure 7: Temporal evolution of the two averaged C-S bonds r_{CS} and both dihedral angles Φ_{SCCS} of TP3, up to 1 ps.

The bond coordinates show a similar behavior as well as the dihedral angles, with no clear preferences. In the first 200 fs only a small part of the trajectories undergo ring-opening and therefore the planarization of TP3 may be considered as the dominant geometrical deformation. After this first period more trajectories show open-ring structures, still accompanied by the out-of-plane vibrational motion around the complete planar structure. Overall, the

bond elongation as well as the inter-ring rotation are less pronounced in the trimer. The *inner* C-S bonds open slightly further than the *central* ones, finally leading to longer time scales for inner bonds elongation.

The position of the first hopping events from the S_1 state into the triplet manifold were also analyzed. In Figure 8 the position of these hopping events are shown depending on the two averaged C-S bonds r_{CS} and both dihedral angles Φ_{SCCS} (see Fig. 1 b)).
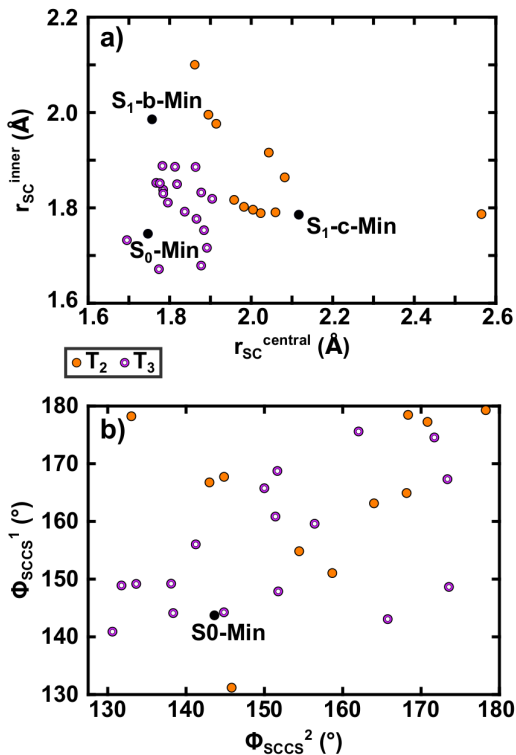
Figure 8: Locations of the TP3 geometries where the first surface hops from the S_1 state to triplet states (T_2 and T_3) occurred depending on both r_{cs} distances (a) and both Φ_{SCCS} dihedral angles (b) for definition see Fig. 1 b). The hopping geometries are displayed in different colors according to the target state of the hopping event. Additionally, relevant B3LYP/DZP optimized geometries are represented in black.

Only intersystem crossing events from the S_1 state into the T_2 and T_3 state are observed. Near the Franck-Condon region, for averaged r_{CS} values between 1.7-1.9 Å, hops to the T_3 state occur. As in the dimer these hops are only intermediate and thus ineffective. Effective hops to the T_2 state are again observed for slightly elongated C-S bonds (1.9-2.2 Å). More hops into the T_2 are observed for *central* bonds longer than 1.9 Å, than for *inner* bonds.

For both Φ_{SCCS} dihedral angles (Fig. 8 b)) no clear trend is observed. T_2-hops occur for dihedral angles in the range 130°-180°. Thus also for TP3 bond elongation is the key process. It enables the intersystem crossing into the triplet states as well as the internal conversion back to the ground state. The energy profiles of four illustrative trajectories are shown in Figure 9.
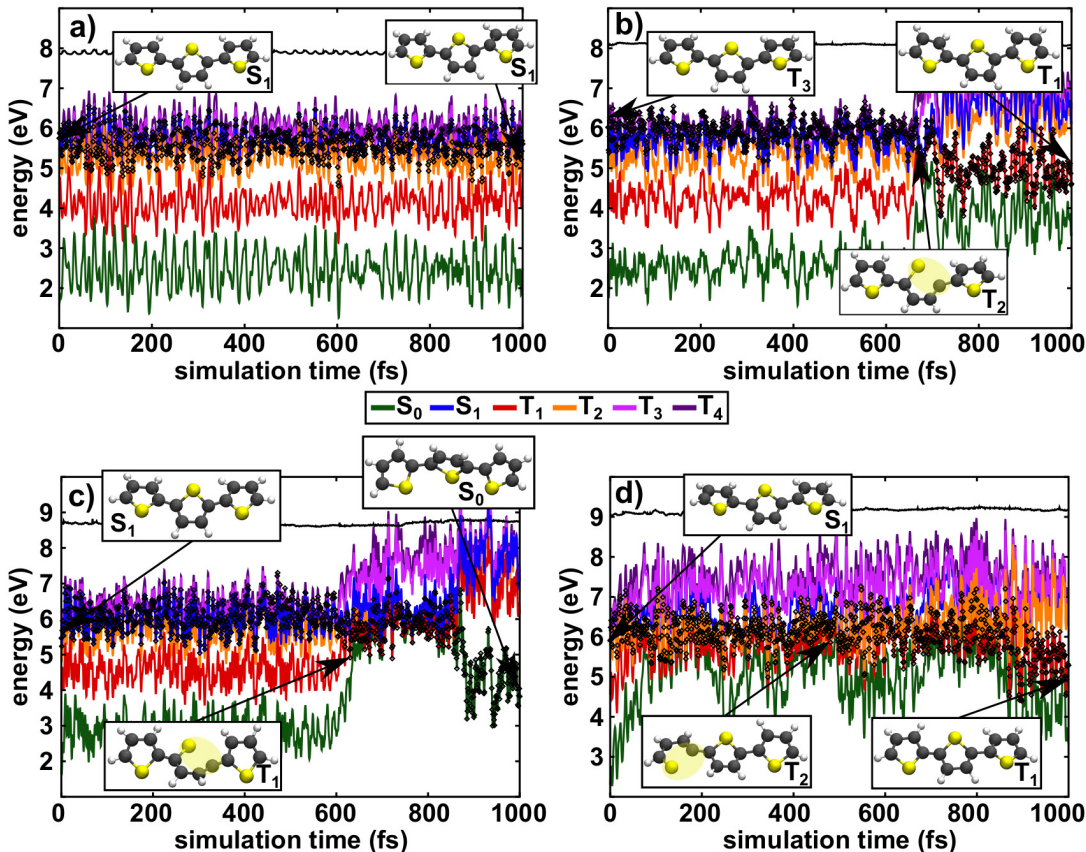
Figure 9: Energy profiles of four representative TP3 trajectories following the ring-opening mechanism. All trajectories were initiated on the S_1 potential energy surface. The time evolution of the ground and the six lowest excited states are displayed in color, whereas the running state is indicated with black diamonds. The energies are plotted relative to the ground state minimum. Example geometries are given for each trajectory, with the broken carbon sulfur bond highlighted in yellow.

The trajectory of Figure 9 a) only shows vibrational dynamics in the S_1 state and presents no non-adiabatic phenomenon. The other trajectories (Figure 9 b), c) and d)) are characterized by intermediate ring-opening events. They can be distinguished either geometrically or regarding their time evolution. In b) and c) one of the *central* C-S bonds is elongated/broken

18

after 600 fs. The resulting open-ring structures survive 10 to 100 fs and form closed-ring structures, respectively, in the T_1 state (b) or the ground state S_0 (c). In the last example d) one of the two *inner* C-S bonds is broken after approximately 100 fs. The resulting open-ring structure persists for about 700 fs allowing hops between the S_1, T_1 and T_2 state. This is in good agreement with the observed slight preference for *inner* bond elongation (compare with Fig. 7 top). The excited state lifetime is globally longer compared to dimer and monomer. This is due to (i) a decrease in spin-orbit couplings as the average C-S bond-elongation is smaller and (ii) an increase in the barrier towards bond elongation. Like the dimer, closed-ring structures are formed in the T_1 state opening the path to phosphorescence.

Conclusions

The relaxation mechanisms of gas-phase irradiated oligothiophene have been unraveled and critically characterized by means of non-adiabatic surface-hopping dynamics. The TDDFT level of theory has been employed to calculate the energies, gradients as well as non-adiabatic and spin-orbit couplings on-the-fly along the trajectories. This level of theory has been carefully benchmarked against high level theoretical as well as experimental data, assuring a qualitatively correct and almost quantitative description of all states involved. In our interpretation we took into account possible limitations of the method in describing the IC back to the ground state. In partial contrast with previous studies performed without the explicit inclusion of the spin-orbit coupling elements, the simulation presents a quite complex scenario in which different competitive pathways are active. Moreover, the influence of the triplet state manifold appears crucial in driving the process. Indeed, in the case of TP2 more than 60 % of the trajectories ends in the triplet manifold after 1ps.

The strong influence of the triplet states was also observed for the case of the thiophene monomer,[24] where it was connected to the carbon sulfur bond cleavage, leading to ring-opening and to a region of singlet triplet quasi-degeneracy and increased spin-orbit couplings. As schematically reported in Figure 10, a similar picture holds also in the case of

oligothiophene, even though the complexity is strongly increased.
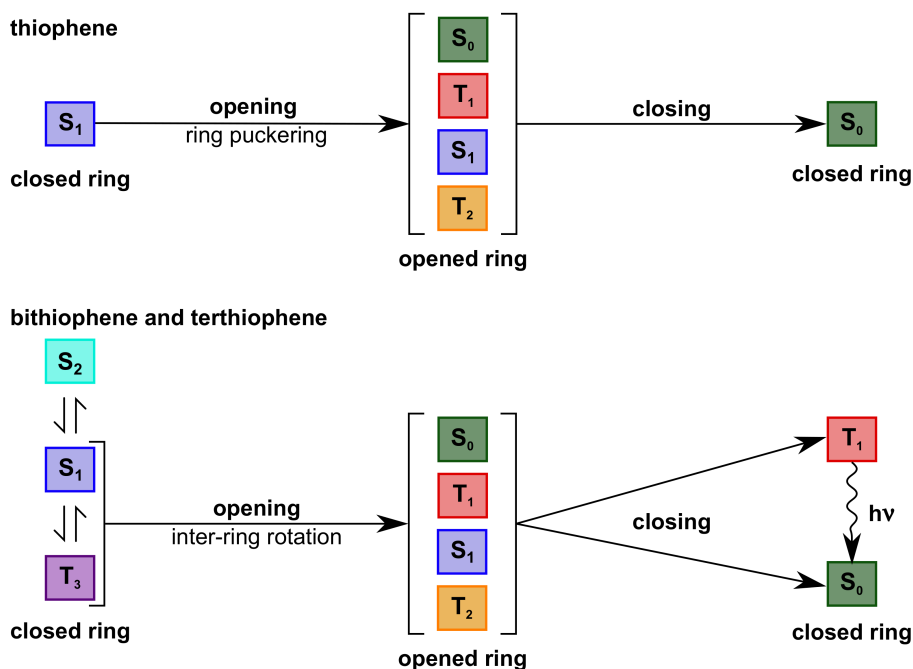
Figure 10: Schematic representation of the pathways active in the excited state relaxation of thiophene monomer compared with bithiophene (TP2) and terthiophene (TP3), as rationalized from non-adiabatic dynamics.

After excitation to the S_1 state, the relaxation process for the majority of the trajectories is described by ring-opening and inter-ring rotation, leading to an extended region of quasi-degeneracy between the triplet and singlet potential energy surfaces. Hence, in this region a complex equilibrium between the different states involved is established, characterized by frequent back and forwards non-adiabatic events. Eventually the system can further evolve to the ring closure that can take place either on the S_0 or the T_1 state. In addition, the ring-opening and subsequent closure is accompanied by a high flexibility of the intermediate molecular systems and indeed *trans-cis* isomerization is observed. The conclusions for the TP3 are qualitatively similar, even if in this case the ring-opening is less pronounced and one should speak of a carbon-sulfur bond elongation rather than of bond-cleavage. With increasing chainlenght the excitation is delocalized over a larger number of bonds, so each individual bond is weakened less.

Our results clearly identify the bond cleavage (or elongation) as the key coordinate driving the relaxation, also via the population of the triplet manifold. This process involves rather large rearrangements of the molecular geometries all along the 1 ps trajectory, even leading to a certain amount of *trans-cis* isomerization. The formation of closed-ring structures in the T_1 state of the dimer and trimer is a prominent difference to the thiophene monomer and we believe it is the reason why phosphorescence is experimentally observable for longer thiophene chains. The efficiency of the ISC is reduced for longer thiophene chains as the driving coordinate, the carbon sulfur bond cleavage, is hindered. Hence, we have provided a consistent description of the photophysics of oligomeric thiophene, taking into account the coupling between intersystem crossing and the geometrical reorganization. However, it has to be underlined that our simulations have been performed in gas phase. The influence of a viscose environment, such as polymeric matrices, can be quite important since the geometric reorganization may be hampered. In the near future we plan to tackle this problem by performing QM/MM non-adiabatic dynamics in thiophene oligomers embedded in rigid polymeric matrices.

Acknowledgement

Supporting Information Available

Validation of the static quantum chemical calculations and comparison with the reference

values. Time series of some relevant geometrical coordinates up to the ps time scale and distribution of the hops between the states. Coordinates of the optimized geometries of the relevant critical points. Evolution of the average population of the states and of the hops between states obtained from the full set of trajectories. This material is available free of charge via the Internet at `http://pubs.acs.org/`.

References

(1) Skotheim, T. A., Reynolds, J. R., Eds. *Handbook of Conducting Polymers*, 3rd ed.; CRC Press: Boca Raton, FL, 2007.

(2) Perepichka, I. F., Perepichka, D. F., Eds. *Handbook of Thiophene-Based Materials: Applications in Organic Electronics and Photonics*; John Wiley & Sons Ltd: Chichester, UK, 2007.

(3) Yu, W.; Donohoo-Vallett, P. J.; Zhou, J.; Bragg, A. E. Ultrafast photo-induced nuclear relaxation of a conformationally disordered conjugated polymer probed with transient absorption and femtosecond stimulated Raman spectroscopies. *J. Chem. Phys.* **2014**, *141*, 044201.

(4) Wang, C.; Angelella, M.; Doyle, S. J.; Lytwak, L. A.; Rossky, P. J.; Holliday, B. J.; Tauber, M. J. Resonance Raman Spectroscopy of the T_1 Triplet Excited State of Oligothiophenes. *J. Phys. Chem. Lett.* **2015**, *6*, 3521–3527.

(5) Thomas, A. K.; Brown, H. A.; Datko, B. D.; Garcia-Galvez, J. A.; Grey, J. K. Interchain Charge-Transfer States Mediate Triplet Formation in Purified Conjugated Polymer Aggregates. *J. Phys. Chem. C* **2016**, *120*, 23230–23238.

(6) Becker, R. S.; Seixas de Melo, J.; Maçanita, A. L.; Elisei, F. Comprehensive Evaluation of the Absorption, Photophysical, Energy Transfer, Structural, and Theoretical

Properties of α-Oligothiophenes with One to Seven Rings. *J. Phys. Chem.* **1996**, *100*, 18683–18695.

(7) Turro, N. J., Ramamurthy, V., Scaiano, J., Eds. *Modern Molecular Photochemistry*, 1st ed.; University Science Books: Mill Valley, CA, 2010.

(8) Rupert, B. L.; Mitchell, W. J.; Ferguson, A. J.; Köse, M. E.; Rance, W. L.; Rumbles, G.; Ginley, D. S.; Shaheen, S. E.; Kopidakis, N. Low-bandgap thiophene dendrimers for improved light harvesting. *J. Mater. Chem.* **2009**, *19*, 5311–5324.

(9) Zhang, F.; Wu, D.; Xu, Y.; Feng, X. Thiophene-based conjugated oligomers for organic solar cells. *J. Mater. Chem.* **2011**, *21*, 17590–17600.

(10) Beaujuge, P. M.; Fréchet, J. M. J. Molecular Design and Ordering Effects in π-Functional Materials for Transistor and Solar Cell Applications. *J. Am. Chem. Soc.* **2011**, *133*, 20009–20029.

(11) Chi, D.; Qu, S.; Wang, Z.; Wang, J. High efficiency P3HT:PCBM solar cells with an inserted PCBM layer. *J. Mater. Chem. C* **2014**, *2*, 4383.

(12) Hu, H.; Jiang, K.; Yang, G.; Liu, J.; Li, Z.; Lin, H.; Liu, Y.; Zhao, J.; Zhang, J.; Huang, F.; Qu, Y.; Ma, W.; Yan, H. Terthiophene-Based D-A Polymer with an Asymmetric Arrangement of Alkyl Chains That Enables Efficient Polymer Solar Cells. *J. Am. Chem. Soc.* **2015**, *137*, 14149–14157.

(13) Gigli, G.; Inganäs, O.; Anni, M.; De Vittorio, M.; Cingolani, R.; Barbarella, G.; Favaretto, L. Multicolor oligothiophene-based light-emitting diodes. *Appl. Phys. Lett.* **2001**, *78*, 1493–1495.

(14) Mazzeo, M.; Pisignano, D.; Favaretto, L.; Barbarella, G.; Cingolani, R.; Gigli, G. Bright oligothiophene-based light emitting diodes. *Synth. Met.* **2003**, *139*, 671–673.

(15) Irie, M.; Fukaminato, T.; Matsuda, K.; Kobatake, S. Photochromism of Diarylethene Molecules and Crystals: Memories, Switches, and Actuators. *Chem. Rev.* **2014**, *114*, 12174–12277.

(16) Barbarella, G.; Zambianchi, M.; Ventola, A.; Fabiano, E.; Della Sala, F.; Gigli, G.; Anni, M.; Bolognesi, A.; Polito, L.; Naldi, M.; Capobianco, M. Bright Oligothiophene N-Succinimidyl Esters for Efficient Fluorescent Labeling of Proteins and Oligonucleotides. *Bioconjugate Chem.* **2006**, *17*, 58–67.

(17) Ho, H.-A.; Najari, A.; Leclerc, M. Optical Detection of DNA and Proteins with Cationic Polythiophenes. *Acc. Chem. Res.* **2008**, *41*, 168–178.

(18) Zambianchi, M.; Maria, F. D.; Cazzato, A.; Gigli, G.; Piacenza, M.; Sala, F. D.; Barbarella, G. Microwave-Assisted Synthesis of Thiophene Fluorophores, Labeling and Multilabeling of Monoclonal Antibodies, and Long Lasting Staining of Fixed Cells. *J. Am. Chem. Soc.* **2009**, *131*, 10892–10900.

(19) Bhaskar, A.; Ramakrishna, G.; Hagedorn, K.; Varnavski, O.; Mena-Osteritz, E.; Bäuerle, P.; Goodson, T. Enhancement of Two-Photon Absorption Cross-Section in Macrocyclic Thiophenes with Cavities in the Nanometer Regime. *J. Phys. Chem. B* **2007**, *111*, 946–954.

(20) Zhou, H.; Zhou, F.; Tang, S.; Wu, P.; Chen, Y.; Tu, Y.; Wu, J.; Tian, Y. Two-photon absorption dyes with thiophene as π-electron bridge: Synthesis, photophysical properties and optical data storage. *Dyes Pigment.* **2012**, *92*, 633–641.

(21) Turan, H. T.; Eken, Y.; Marazzi, M.; Pastore, M.; Aviyente, V.; Monari, A. Assessing One- and Two-Photon Optical Properties of Boron Containing Arenes. *J. Phys. Chem. C* **2016**, *120*, 17916–17926.

(22) Huix-Rotllant, M.; Tamura, H.; Burghardt, I. Concurrent Effects of Delocalization and

Internal Conversion Tune Charge Separation at Regioregular Polythiophene-Fullerene Heterojunctions. *J. Phys. Chem. Lett.* **2015**, *6*, 1702–1708.

(23) Kölle, P.; Schnappinger, T.; de Vivie-Riedle, R. Deactivation pathways of thiophene and oligothiophenes: internal conversion versus intersystem crossing. *Phys. Chem. Chem. Phys.* **2016**, *18*, 7903–7915.

(24) Schnappinger, T.; Kölle, P.; Marazzi, M.; Monari, A.; González, L.; de Vivie-Riedle, R. Ab initio molecular dynamics of thiophene: the interplay of internal conversion and intersystem crossing. *Phys. Chem. Chem. Phys.* **2017**, *19*, 25662–25670.

(25) Weinkauf, R.; Lehr, L.; Schlag, E. W.; Salzmann, S.; Marian, C. M. Ultrafast dynamics in thiophene investigated by femtosecond pump probe photoelectron spectroscopy and theory. *Phys. Chem. Chem. Phys.* **2008**, *10*, 393–404.

(26) Lap, D. V.; Grebner, D.; Rentsch, S. Femtosecond Time-Resolved Spectroscopic Studies on Thiophene Oligomers. *J. Phys. Chem. A* **1997**, *101*, 107–112.

(27) Paa, W.; Yang, J.-P.; Rentsch, S. Intersystem crossing in oligothiophenes studied by fs time-resolved spectroscopy. *Appl. Phys. B* **2000**, *71*, 443–449.

(28) Barclay, M. S.; Quincy, T. J.; Williams-Young, D. B.; Caricato, M.; Elles, C. G. Accurate Assignments of Excited-State Resonance Raman Spectra: A Benchmark Study Combining Experiment and Theory. *J. Phys. Chem. A* **2017**, *121*, 7937–7946.

(29) Rubio, M.; Merchán, M.; Ortí, E.; Roos, B. O. A theoretical study of the electronic spectrum of bithiophene. *J. Chem. Phys.* **1995**, *102*, 3580.

(30) Rubio, M.; Merchán, M.; Pou-Amérigo, R.; Ortí, E. The Low-Lying Excited States of 2,2'-Bithiophene: A Theoretical Analysis. *ChemPhysChem* **2003**, *4*, 1308–1315.

(31) Rubio, M.; Merchán, M.; Ortí, E. A Theoretical Study on the Low-Lying Excited States

of 2,2':5',2"-Terthiophene and 2,2':5',2":5",2"'-Quaterthiophene. *ChemPhysChem* **2005**, *6*, 1357–1368.

(32) Siegert, S.; Vogeler, F.; Marian, C. M.; Weinkauf, R. Throwing light on dark states of α-oligothiophenes of chain lengths 2 to 6: radical anion photoelectron spectroscopy and excited-state theory. *Phys. Chem. Chem. Phys.* **2011**, *13*, 10350–10363.

(33) Fazzi, D.; Barbatti, M.; Thiel, W. Modeling ultrafast exciton deactivation in oligothiophenes via nonadiabatic dynamics. *Phys. Chem. Chem. Phys.* **2015**, *17*, 7787–7799.

(34) Prlj, A.; Curchod, B. F. E.; Corminboeuf, C. Excited state dynamics of thiophene and bithiophene: new insights into theoretically challenging systems. *Phys. Chem. Chem. Phys.* **2015**, *17*, 14719–14730.

(35) Lin, J. B.; Jin, Y.; Lopez, S. A.; Druckerman, N.; Wheeler, S. E.; Houk, K. N. Torsional Barriers to Rotation and Planarization in Heterocyclic Oligomers of Value in Organic Electronics. *J. Chem. Theory Comput.* **2017**, *13*, 5624–5638.

(36) Richter, M.; Marquetand, P.; González-Vázquez, J.; Sola, I.; González, L. SHARC: ab initio Molecular Dynamics with Surface Hopping in the Adiabatic Representation Including Arbitrary Couplings. *J. Chem. Theory Comput.* **2011**, *7*, 1253–1258.

(37) Mai, S.; Marquetand, P.; González, L. A General Method to Describe Intersystem Crossing Dynamics in Trajectory Surface Hopping. *Int. J. Quantum Chem.* **2015**, *115*, 1215–1231.

(38) Mai, S.; Marquetand, P.; González, L. Nonadiabatic dynamics: The SHARC approach. *Wiley Interdiscip. Rev.: Comput. Mol. Sci.* **2018**, *0*, e1370.

(39) Mai, S.; Richter, M.; Heindl, M.; Menger, M. F. S. J.; Atkins, A.; Ruckenbauer, M.; Plasser, F.; Oppel, M.; Marquetand, P.; González, L. SHARC2.0: Surface Hopping

26

Including Arbitrary Couplings - Program Package for Non-Adiabatic Dynamics. sharc-md.org, 2018.

(40) Richter, M.; Mai, S.; Marquetand, P.; González, L. Ultrafast intersystem crossing dynamics in uracil unravelled by ab initio molecular dynamics. *Phys. Chem. Chem. Phys.* **2014**, *16*, 24423–24436.

(41) Cao, J.; Xie, Z.-Z.; Yu, X. Excited-state dynamics of oxazole: A combined electronic structure calculations and dynamic simulations study. *Chem. Phys.* **2016**, *474*, 25 – 35.

(42) Marazzi, M.; Mai, S.; Roca-Sanjuán, D.; Delcey, M. G.; Lindh, R.; González, L.; Monari, A. Benzophenone Ultrafast Triplet Population: Revisiting the Kinetic Model by Surface-Hopping Dynamics. *J. Phys. Chem. Lett.* **2016**, *7*, 622–626.

(43) Mai, S.; Pollum, M.; Martínez-Fernández, L.; Dunn, N.; Marquetand, P.; Corral, I.; Crespo-Hernández, C. E.; González, L. The origin of efficient triplet state population in sulfur-substituted nucleobases. *Nat. Commun.* **2016**, *7*, 13077.

(44) Mai, S.; Marquetand, P.; González, L. Intersystem Crossing Pathways in the Noncanonical Nucleobase 2-Thiouracil: A Time-Dependent Picture. *J. Phys. Chem. Lett.* **2016**, *7*, 1978–1983.

(45) Hirata, S.; Head-Gordon, M. Time-dependent density functional theory within the Tamm-Dancoff approximation. *Chem. Phys. Lett.* **1999**, *314*, 291–299.

(46) Baerends, E. J. et al. ADF2017, SCM, Theoretical Chemistry, Vrije Universiteit, Amsterdam, The Netherlands, https://www.scm.com.

(47) te Velde, G.; Bickelhaupt, F. M.; Baerends, E. J.; Fonseca Guerra, C.; van Gisbergen, S. J. A.; Snijders, J. G.; Ziegler, T. Chemistry with ADF. *J. Comput. Chem.* **2001**, *22*, 931–967.

(48) Lee, C.; Yang, W.; Parr, R. G. Development of the Colle-Salvetti correlation-energy formula into a functional of the electron density. *Phys. Rev. B* **1988**, *37*, 785–789.

(49) Becke, A. D. Density-functional thermochemistry. III. The role of exact exchange. *J. Chem. Phys.* **1993**, *98*, 5648–5652.

(50) Stephens, P. J.; Devlin, F. J.; Chabalowski, C. F.; Frisch, M. J. Ab Initio Calculation of Vibrational Absorption and Circular Dichroism Spectra Using Density Functional Force Fields. *J. Chem. Phys.* **1994**, *98*, 11623–11627.

(51) Grimme, S.; Antony, J.; Ehrlich, S.; Krieg, H. A consistent and accurate ab initio parametrization of density functional dispersion correction (DFT-D) for the 94 elements H-Pu. *J. Chem. Phys.* **2010**, *132*, 154104.

(52) Neese, F. The ORCA program system. *Wiley Interdiscip. Rev.: Comput. Mol. Sci.* **2012**, *2*, 73–78.

(53) Van Lenthe, E.; Baerends, E. J. Optimized Slater-type basis sets for the elements 1-118. *J. Comput. Chem.* **2003**, *24*, 1142–1156.

(54) Becke, A. D. A multicenter numerical integration scheme for polyatomic molecules. *J. Chem. Phys.* **1988**, *88*, 2547–2553.

(55) Franchini, M.; Philipsen, P. H. T.; Visscher, L. The Becke Fuzzy Cells Integration Scheme in the Amsterdam Density Functional Program Suite. *J. Comput. Chem.* **2013**, *34*, 1819–1827.

(56) Franchini, M.; Philipsen, P. H. T.; van Lenthe, E.; Visscher, L. Accurate Coulomb Potentials for Periodic and Molecular Systems through Density Fitting. *J. Chem. Theory Comput.* **2014**, *10*, 1994–2004.

(57) van Lenthe, E.; Baerends, E. J.; Snijders, J. G. Relativistic regular two-component Hamiltonians. *J. Chem. Phys.* **1993**, *99*, 4597–4610.

(58) van Lenthe, E.; Baerends, E. J.; Snijders, J. G. Relativistic total energy using regular approximations. *J. Chem. Phys.* **1994**, *101*, 9783–9792.

(59) van Lenthe, E.; Snijders, J. G.; Baerends, E. J. The zero-order regular approximation for relativistic effects: The effect of spin-orbit coupling in closed shell molecules. *J. Chem. Phys.* **1996**, *105*, 6505–6516.

(60) van Lenthe, E.; van Leeuwen, R.; Baerends, E. J.; Snijders, J. G. Relativistic regular two-component Hamiltonians. *Int. J. Quantum Chem.* **1996**, *57*, 281–293.

(61) van Lenthe, E.; Ehlers, A.; Baerends, E.-J. Geometry optimizations in the zero order regular approximation for relativistic effects. *J. Chem. Phys.* **1999**, *110*, 8943–8953.

(62) Wang, F.; Ziegler, T. A simplified relativistic time-dependent density-functional theory formalism for the calculations of excitation energies including spin-orbit coupling effect. *J. Chem. Phys.* **2005**, *123*, 154102.

(63) Duarte, H. A.; Dos Santos, H. F.; Rocha, W. R.; De Almeida, W. B. Improved quantum mechanical study of the potential energy surface for the bithiophene molecule. *J. Chem. Phys.* **2000**, *113*, 4206–4215.

(64) Ciofalo, M.; Manna, G. L. Ab initio conformational study of 2,2':5',2"-terthiophene. *Chem. Phys. Lett.* **1996**, *263*, 73–78.

(65) Millefiori, S.; Alparone, A.; Millefiori, A. Conformational properties of thiophene oligomers. *J. Heterocyclic Chem.* **2000**, *37*, 847–853.

(66) Liu, F.; Zuo, P.; Meng, L.; Zheng, S. J. On the optical properties of thiophene oligomers: configuration interaction study on their ground (S_0) and first singlet excited (S_1) states. *THEOCHEM* **2005**, *726*, 161–169.

(67) Mai, S.; Marquetand, P.; Richter, M.; González-Vázquez, J.; González, L. Singlet and

Triplet Excited-State Dynamics Study of the Keto and Enol Tautomers of Cytosine. *ChemPhysChem* **2013**, *14*, 2920–2931.

(68) Granucci, G.; Persico, M.; Toniolo, A. Direct semiclassical simulation of photochemical processes with semiempirical wave functions. *J. Chem. Phys.* **2001**, *114*, 10608–10615.

(69) Plasser, F.; Ruckenbauer, M.; Mai, S.; Oppel, M.; Marquetand, P.; González, L. Efficient and Flexible Computation of Many-Electron Wave Function Overlaps. *J. Chem. Theory Comput.* **2016**, *12*, 1207–1219.

(70) Granucci, G.; Persico, M. Critical appraisal of the fewest switches algorithm for surface hopping. *J. Chem. Phys.* **2007**, *126*, 134114.

(71) Belletête, M.; Leclerc, M.; Durocher, G. Potentialities of Semiempirical Calculations (AMPAC and INDO/S) in Determining the Conformation and Electronic Properties of 2,2'-Bithiophene: A New Joint Experimental and Theoretical Approach. *J. Phys. Chem.* **1994**, *98*, 9450–9456.

(72) Grebner, D.; Helbig, M.; Rentsch, S. Size-Dependent Properties of Oligothiophenes by Picosecond Time-Resolved Spectroscopy. *J. Phys. Chem.* **1995**, *99*, 16991–16998.

(73) DiCésare, N.; Belletête, M.; Marrano, C.; Leclerc, M.; Durocher, G. Intermolecular Interactions in Conjugated Oligothiophenes. 1. Optical Spectra of Terthiophene and Substituted Terthiophenes Recorded in Various Environments. *J. Phys. Chem. A* **1999**, *103*, 795–802.

(74) Crespo-Otero, R.; Barbatti, M. Recent Advances and Perspectives on Nonadiabatic Mixed Quantum-Classical Dynamics. *Chemical Reviews* **0**, *0*, null, PMID: 29767966.

(75) Rentsch, S.; Yang, J. P.; Paa, W.; Birckner, E.; Schiedt, J.; Weinkauf, R. Size dependence of triplet and singlet states of α-oligothiophenes. *Phys. Chem. Chem. Phys.* **1999**, *1*, 1707–1714.

Graphical TOC Entry